Thermopower and magnetotransport properties of $Bi_{100-x}Sb_x$ topological insulator thin films prepared by flash evaporation

E. Osmic,[1, *] J. Barzola-Quiquia,[1] W. Böhlmann,[1] P. G. Bercoff,[2] L. Venosta,[2] and P. Häussler[3]

[1] *Felix-Bloch Institute for Solid-state Physics, University of Leipzig, 04103 Leipzig, Germany*

[2] *Universidad Nacional de Córdoba, Facultad de Matemática, Astronomía, Física y Computación (FAMAF).*
Instituto de Física Enrique Gaviola (IFEG), CONICET.
Av. Medina Allende s/n, 5000 Córdoba, Argentina

[3] *Division of Thin Films Physics, Institute of Physics,*
Chemnitz University of Technology, 09107 Chemnitz, Germany

(Dated: February 11, 2022)

We have measured the temperature dependence of resistance $R(T)$, thermopower $S(T)$, magnetoresistance (MR) and the Hall effect (HE) of $Bi_{80}Sb_{20}$, $Bi_{85}Sb_{15}$ and $Bi_{90}Sb_{10}$ topological insulator thin films. Samples were prepared by sequential flash-evaporation at room temperature and annealing at $T = 350\,K$. The $R(T)$ of the three investigated samples show metallic-like behavior for temperatures less than $T = 75\,K$, while at higher temperatures, $R(T)$ curves show a semiconducting-like behavior. The thermopower $S(T)$ of the three investigated samples is negative in the entire temperature range measured in this work, with a linear behavior from 5 up to $\approx 100\,K$. The magnetoresistance of all samples is positive with a small temperature dependence. The highest $MR(B = 7\,T)$ was observed in $Bi_{85}Sb_{15}$ with a $\approx 600\,\%$ and $\approx 125\,\%$ change at 5 and 300 K, respectively. Clear evidence of weak antilocalization contribution to the MR was observed only in sample $Bi_{85}Sb_{15}$ for temperatures $T < 75\,K$. Quantum oscillations in the MR originating from the Fermi surface, which has a clear two-dimensional character, were observed in sample $Bi_{85}Sb_{15}$ up to $\approx 21\,K$. Carrier mobility information of sample $Bi_{85}Sb_{15}$ was extracted from low field HE data, showing a remarkably high value of $\mu \approx 2.8 \times 10^4$ cm^2/Vs at 5 K, with a small decrease for increasing temperature.

I. INTRODUCTION

Three-dimensional (3D) topological insulators (TI) are a new class of materials with a bulk gap generated by the spin-orbit interaction and the presence of gapless metallic surface states [1,2]. The theory predicts that the surface states are topologically protected, which means that they are robust against disorder and magnetic impurities [3]. In 2007, the existence of 3D TI materials [1,2,4] was theoretically predicted and in the same year the small-gap semiconducting alloys $Bi_{100-x}Sb_x$, α-Sn and HgTe (under uniaxial strain) were proposed as candidates by Fu and Kane [2]. The first 3D topological insulator to be experimentally discovered was the alloy $Bi_{100-x}Sb_x$, the unusual surface bands of which were mapped in an angle-resolved photoemission spectroscopy (ARPES) experiment [5,6]. After the discovery of $Bi_{100-x}Sb_x$ surface states, the search for TI materials has lead to the discovery of TI behavior in Bi_2Se_3 [7,8], Sb_2Te_3 [8] and Bi_2Te_3 [8,9]. TI materials are promising for future potential applications in spintronics [10], superconductivity [11], quantum computing [12], etc. Besides $Bi_{100-x}Sb_x$ being recently recognized as a TI material, $Bi_{100-x}Sb_x$ alloys have been studied since many decades ago because of their remarkable electronic transport properties, when considered as a function of stoichiometry, temperature, strain, pressure, magnetic field, etc [13–16]. Also, $Bi_{100-x}Sb_x$ alloys are known as some of the best thermoelectric materials with a high thermoelectric figure of merit Z. Therefore,

they are currently used for applications and consequently have been studied in great detail [14–16]. After the verification of TI behavior by means of ARPES experiments, the first report (to the best of our knowledge) on the transport properties of $Bi_{100-x}Sb_x$ showing TI behavior was done by Taskin and Ando [17]. They observed strong quantum oscillations in the magnetization and the resistivity of $Bi_{100-x}Sb_x$ crystals originated from a Fermi surface with a clear two-dimensional character [17,18]. Magnetoresistance showing weak anti-localization (WAL) is used as evidence that the electrons moving at the surface of the material are time-reversal symmetry protected. In a TI the WAL effect is a result of the strong spin-orbit coupling, which, in the presence of defects, minimizes the backscattering when a magnetic field or magnetic impurities are not present. In the absence of localization, the surface of a TI remains metallic and it is expected to exhibit perfect WAL due to helical surface states [19,20]. Therefore, 2D WAL was used to verify the topological nature in several cases [21–24], where the temperature dependence of the coherence length l_ϕ can be used to prove that the WAL originates from the 2D surface states. The observation of WAL in TI $Bi_{100-x}Sb_x$ is difficult because of the bulk contribution to the conductivity at all temperatures. However, Maurya *et al.* [25] have recently observed a dramatic increase in the magnetoresistance when measuring bulk crystals in a low magnetic-field range, finding that MR becomes linear at higher fields, which indicates the presence of WAL.

For future applications in the micro and nanotech-

nology, tremendous efforts are being done in order to produce this kind of materials as thin films, nanowires, nanocrystals etc., using different techniques such as molecular beam epitaxy (MBE)[26,27], metal-organic chemical vapour deposition[28], mechanical exfoliation as done in graphene[29,30], an improved Ulitovsky method[31] or chemical vapour transport[32]. Nevertheless, the preparation of large area $Bi_{100-x}Sb_x$ films and the possibility to obtain a variety of morphologies by the combination of electron beam lithography techniques is still a challenge.

In this work, we have used a simple and powerful technique to produce $Bi_{100-x}Sb_x$ thin films, i.e. sequential flash evaporation[33] (SFE), a method which has been successfully used to produce high quality thin films of the topological insulator $Bi_{40}Se_{60}$[24] and another exotic materials such as quasicrystals[34–37] and Heusler alloys[38]. SFE has advantages not only because of its simplicity, but also because it allows the production of homogeneous centimeter-sized samples. The simultaneous measurement of the different electrical transport properties reported here was possible because of the combination of SFE and electron beam lithography. The results presented in this work show very good agreement with previous papers on TI $Bi_{100-x}Sb_x$ and provide new insights on the electrical properties of this alloy.

II. EXPERIMENTAL DETAILS

BiSb alloys were prepared by melting pure bismuth and antimony (purity 99.9999%) in proper atomic proportions in an evacuated quartz ampoule at a base pressure of approximately $P \approx 10^{-7}$ mbar. After the alloy was removed from the ampoule and milled into pieces of 200–300 µm in diameter, it was introduced into the flash evaporation device. The flash evaporation process was performed at room temperature under a nominal pressure of $\approx 5 \times 10^{-7}$ mbar on different substrates, obtaining ∼100 nm thick films. The atomic composition, the lattice parameters and orientation of the produced samples were determined by energy-dispersive X-ray spectroscopy (EDX) and X-ray Laue diffraction, respectively. The results confirm the purity and nominal composition of the samples as well as the crystalline structure, and they are presented in the supplementary information (SI). For thermopower measurements the substrates were thin glass slides, which were glued onto the sample holder to achieve good thermal contact. On the other hand, for resistance measurements, the films were prepared onto Si substrates ($5 \times 5 \times 0.5$ mm^3) caped with 500 nm SiO$_2$. The resistance was measured using the 4-point probe method with two additional contacts for Hall effect (HE) which were designed using electron beam lithography. The absolute Seebeck coefficient $S(T)$ was measured between 5 and 325 K by applying a slowly alternating temperature gradient across the thin films[39]. The advantage of this dynamical method is the suppression of spurious EMFs
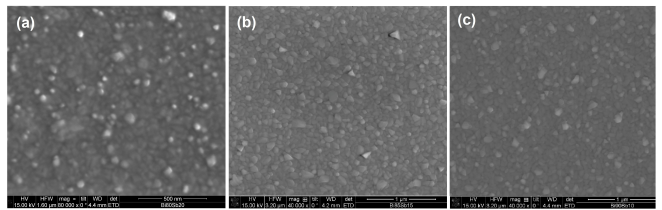

Fig. 1. SEM images of the investigated samples. Figures (a)-(c) correspond to samples $Bi_{80}Sb_{20}$, $Bi_{85}Sb_{15}$ and $Bi_{90}Sb_{10}$, respectively. The scale in the images corresponds to 500 nm.

and offset drifts, i.e. high resolution. The thermo-emfs were amplified by means of a Keithley nanovoltmeter 182 with a resolution of 1 nV. The temperature dependence of resistance $R(T)$, magnetoresistance and Hall effect were measured between 5 K and 325 K in a commercial ^{4}He cryostat equipped with a ± 7 Tesla superconducting magnet. The low-noise resistance measurements were performed using the AC technique (Linear Research LR-700 Bridge) with high resolution.

III. RESULTS AND DISCUSSION

Scanning electron microscope (SEM) measurements were performed in order to get information about the crystal size and surface morphology of the prepared films. According to the SEM images displayed in Fig. 1, the average crystal sizes after annealing up to 345 K are in the order of ≈ 50 nm, ≈ 55 nm and ≈ 57 nm for samples $Bi_{80}Sb_{20}$, $Bi_{85}Sb_{15}$ and $Bi_{90}Sb_{10}$, respectively. According to our Laue diffraction results shown in the SI, the lattice parameters are in good agreement with those reported in the literature[40] and the crystals are oriented with the c-axis perpendicular to the substrate. EDX results (presented in the SI) show that the estimated concentration deviates $\approx 1\%$ from the nominal composition. A relevant result from EDX analysis is that our samples don't contain any ferromagnetic contaminants (such as Fe, Ni and Co) within the detection limit of the technique. We can conclude that with our preparation method and after annealing, we have produced polycrystalline films of great purity and controlled composition. The estimated crystal sizes are in agreement with those from the literature for samples with similar preparation methods and thermal treatments[41,42].

A. Temperature dependence of the resistance

Resistance measurements as a function of temperature of the three investigated samples are presented in Fig. 2 in a normalized form, i.e. $R_N(T) = R(T)/R(T = 325\,K)$. At temperatures lower than ≈ 75 K the resistance displays a metallic behavior in the three samples, while for temperatures above this value, a semiconducting-like be-
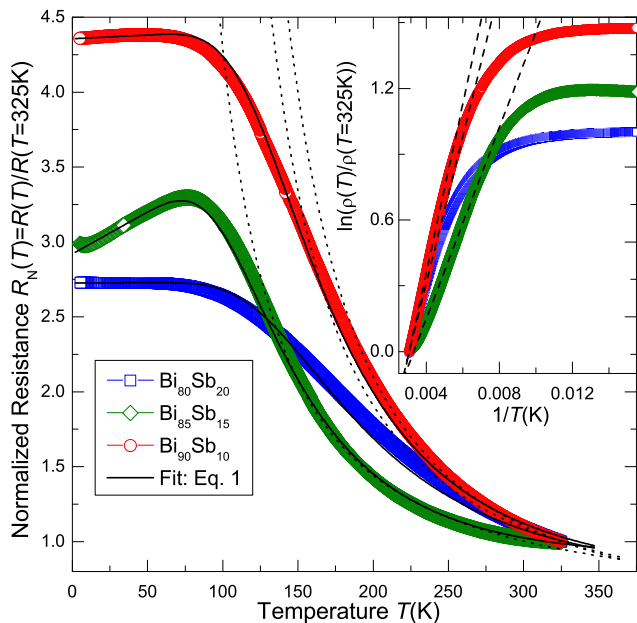
Fig. 2. Normalized resistance of the investigated samples are shown as open symbols, the lines are the corresponding fits using the model discussed in the main text. The inset shows the usual method used in the literature to calculate the gap energy of similar samples to ours. The dotted lines in the main figure are calculated using the equation $\rho(T) = \rho_a \exp(E_{go}/2k_B T)$, with E_{go} obtained from the inset.

havior is observed, being in good agreement with other works [17,42,43].

In order to obtain further information about the metallic and semiconducting contributions to the estimated resistivity $\rho(T)$, we have used a model proposed in Ref.[44] which describes the resistivity as a function of temperature $\rho(T)$ of few layers of graphene, a material with similar $\rho(T)$[45,46] and magneto-transport properties than TI materials. The model considers that the total resistivity $\rho_F(T)$ (where the subscript F corresponds to the fitting model) is a result of a parallel contribution from a metallic resistivity ρ_M and a semiconducting resistivity ρ_S as follows:

$$\rho_F(T)^{-1} = \rho_M(T)^{-1} + \rho_S(T)^{-1}, \qquad (1)$$

with

$$\rho_M(T) = \rho_0 + \rho_1 T, \qquad (2)$$

and

$$\rho_S(T) = a_0 T^{3/2} \exp(E_g/2k_B T), \qquad (3)$$

where k_B is the Boltzmann constant, the coefficients ρ_0, ρ_1 and a_0, as well as the semiconducting band gap E_g are free parameters. More detailed explanation about the model itself can be found in Ref.[44,47,48]. In our specific case, the first term in Eq.1 describes the metallic
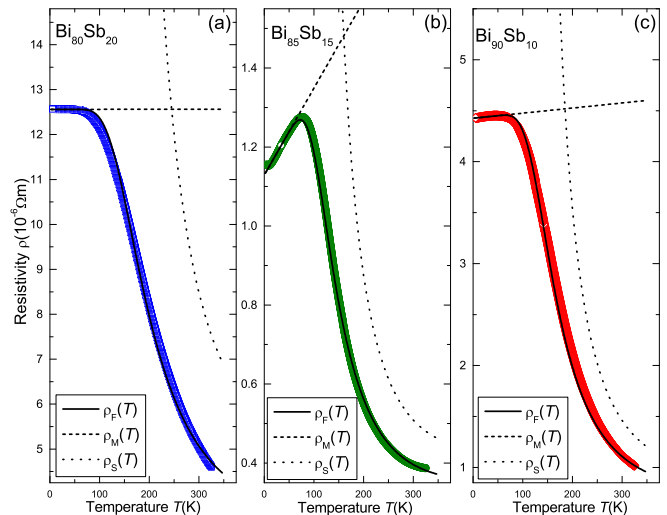

Fig. 3. Temperature dependence of the resistivity $\rho(T)$ and the fits obtained using Eq.1 (solid lines). The corresponding contributions given by Eq.2 (dashed lines) and Eq.3 (dotted lines) are also displayed.

contribution due to the metallic states at the surface of the formed crystals in the thin film, and the second term in Eq.1 comes from the bulk state of the crystals. The parameters obtained after fitting the experimental $\rho(T)$ are listed in Table I.

The fit results using the model described by Eq.1 are quite accurate at all temperatures, as shown by the solid lines in Fig.2 and Fig.3, so we can conclude that the model describes very well the experimental results across the entire range of investigated temperatures.

From the results associated with the metallic contribution we can observe that the parameter ρ_0 –related to the residual resistivity– is smaller for sample $Bi_{85}Sb_{15}$ compared to the others, while the parameter ρ_1 –related to the linear metallic contribution– is a couple of orders greater than in the other samples, reflecting the metallic character of $Bi_{85}Sb_{15}$ in a broad range of temperatures. The semiconducting contribution can be compared to very well-known results for bulk and thin films. Surprisingly, the E_g values obtained from the fits using Eq.1 are in disagreement with experimental results from other authors [14,15,42,49,50] in all three cases. In order to un-

TABLE I. Parameters ρ, ρ_1 and a_0, and semiconducting band gap E_g, obtained from the fitting of experimental data with Eqs.(1) - (3). Semiconducting band gap E_{go}, from the fit with Eq.(4).

Sample	ρ_0 ($\mu\Omega$m)	ρ_1 ($\mu\Omega$m/K)	a_0 ($\mu\Omega$m/T$^{1.5}$)	E_g (meV)	E_{go} (meV)
$Bi_{80}Sb_{20}$	12.56	0.000011	0.0000736	157	57.7
$Bi_{85}Sb_{15}$	1.129	0.0022	0.0000098	119	37.6
$Bi_{90}Sb_{10}$	4.426	0.0005	0.0000142	154	66.4

derstand the origin of this difference, we have applied a widely-used method to calculate the band gap, i.e. to plot the logarithm of the normalized resistance vs. the inverse of temperature (see the inset in Fig. 2). From the linear fit of the experimental data, using the equation

$$\rho(T) = \rho_a \exp(E_{go}/2k_{\mathrm{B}}T),\qquad(4)$$

where ρ_a ia a prefactor, we have determined the band gap E_{go}. The so-obtained E_{go} values are listed in Table I and –as it can be readily seen– in this case these values agree with the reported band-gap values for BiSb alloys [14,15,42,49,50]. The difference between E_g and E_{go} can be related to the fact that by applying the traditionally used method to calculate the band gap (Eq. 4), only a small region of the $R(T)$ curve is considered. This statement is evident in Fig. 2, where the dotted lines correspond to the fits using the mentioned method and it is clear that the agreement with the experimental data is good only for temperatures above $\sim 150 - 200$ K. Since $\rho(T)$ curves fitted with an adequate model in a broad temperature range have not yet been reported for this kind of materials, we have plotted in Fig. 3 the experimental resistivity $\rho(T)$ together with the fit using Eq. 1 and the corresponding metallic (ρ_M) and semiconducting (ρ_S) contributions, using Eq. 2 and Eq. 3, respectively. In Fig. 3, the solid lines correspond to the $\rho_F(T)$ results, the dashed lines to the metallic contribution $\rho_M(T)$ and the dotted lines to the semiconducting contribution $\rho_S(T)$. From the fittings we can observe that the rest resistivity, i.e. $\rho_M(T = 0) = \rho_0$ has a high value for sample $Bi_{80}Sb_{20}$, followed by $Bi_{90}Sb_{10}$ and the smallest value is attained by sample $Bi_{85}Sb_{15}$. The fact that $\rho_M(T = 0)$, for sample $Bi_{85}Sb_{15}$ is small compared to the others, indicates that in this case the metallic states formed at the grains surface are more robust than the defects present at the grains surface itself. In order to compare our results with those from other authors, we have listed in Table II the rest resistivity ρ_0 data of our samples. Here, it can be observed that our values for $Bi_{85}Sb_{15}$ are in agreement with previous results, indicating the high quality of the samples obtained with our preparation method. Usually, when the resistance of a metal is described, the following equation is used, $\rho(T) = \rho_b[1 + \alpha(T - T_b)]$, being ρ_b the resistivity at temperature $T = T_b$ and α the so-called temperature coefficient of the resistance. The α coefficients estimated for our samples (listed in Table II) are in agreement with those from other results for similar TI Bi_xSb_{100-x} films; they are also comparable to the α of other TI, such as Bi_2Se_3. For comparison, different data from the literature are listed in Table II. We interpret the fact that the metallic contribution in samples $Bi_{80}Sb_{20}$ and $Bi_{90}Sb_{10}$ are almost temperature-independent as a consequence of the metallic states formed at the surface of both samples, being less robust to the scattering produced by defects and/or impurities. We find it remarkable that the highest α is obtained for sample $Bi_{85}Sb_{15}$, which we interpret as

the sample with the best metallic state at the surface when compared to the others. Hence, for this particular composition we can expect a special behavior when an external magnetic field is applied.

B. Thermopower and power factor

Fig. 4 shows the thermopower $S(T)$ curves measured for the three investigated samples, which display negative values in the entire temperature range. From the lowest temperature up to $T \approx 100$ K, $S(T)$ behaves linearly with a negative slope, then it reaches a minimum and changes to a positive slope. For the complete temperature range, the largest $S(T)$ values are attained by samples $Bi_{85}Sb_{15}$ and $Bi_{90}Sb_{10}$. Seemingly, the linearity in the thermopower can be interpreted as a consequence of a dominant electron-phonon scattering process, like in pure metals.

The expression for the thermopower in the free electron model is

$$S_D(T) = -\pi^2 k_B^2 T/|e|E_F,\qquad(5)$$

where E_F is the Fermi energy, e is the electron charge and k_{B} is the Boltzman constant. This equation was used to fit the experimental data of $S(T)$ for the three samples and the results are shown as solid lines in Fig. 4 for temperatures below the Debye temperature θ_D, which was calculated using the Kopp-Neumann relation:

$$\theta_{D-Bi_{1-x}Sb_x}^{-3} = (1 - x)\,\theta_{D-Bi}^{-3} + x\,\theta_{D-Sb}^{-3},\qquad(6)$$

being θ_{D-Bi} and θ_{D-Sb} the Debye temperatures of Bi and Sb, respectively. The obtained E_F are listed in Table III, together with the Fermi energies E_{F0} calculated using the free electron model. The great discrepancies between E_F and E_{F0} indicate that the linear thermopower observed in our samples at $T < \theta_D$ has a more complicated scattering mechanism than the electron-phonon scattering.

It is clear that the semi-classical Boltzmann transport theory in the framework of constant relaxation time

TABLE II. Data from this work (*) compared with data from the literature for similar materials.

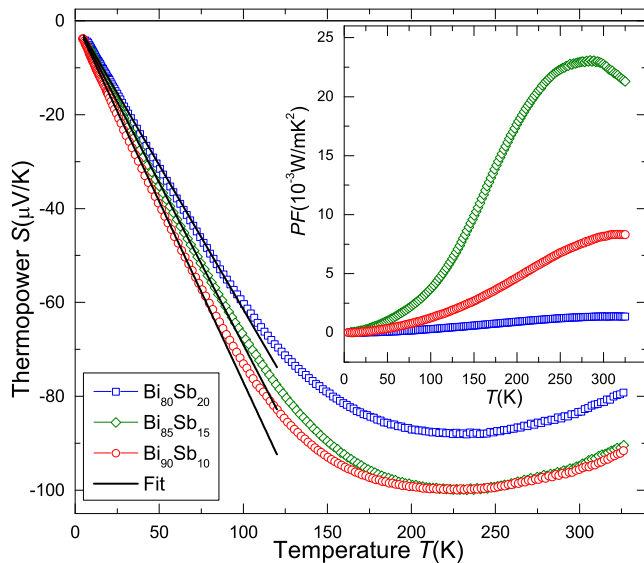| Parameter	$Bi_{80}Sb_{20}$	$Bi_{85}Sb_{15}$	$Bi_{90}Sb_{10}$	Bi_2Se_3
$\rho_0(\mu\Omega m)$	12.56*, 1.75[14], 4.4[49]	1.29*, 1.65[14], 2.05[15], 2.3[49], 17.1[42]	4.42*, 1.55[14], 2.53[49], 2.9[17], 14.1[42]	7[51], 25[52]
$\alpha(10^{-4}$/K)	0.015*, 13[49]	22*, 192.7[15], 23.2[49], 1.95[42]	1.6*, 2.5[49], 20.1[17], 0.23[42]	31.9[51], 8.8[24]

Fig. 4. Temperature dependence of the thermopower $S(T)$ after annealing at $T = 350$ K. The solid lines correspond to the fits using Eq. 5. The inset displays the calculated power factor $PF(T)$ of our samples.

Fig. 5. Magnetoresistance (a) and Hall resistance (b) of sample $Bi_{80}Sb_{20}$.

(τ) —which is the most frequently used for conventional analysis of the thermopower in metals and small gap semiconductors— cannot be valid in the analysis of 3D topological insulators, where a strong energy dependent relaxation time $\tau(E)$ is expected, beyond the Born approximation (as it was proposed by Tretiakov *et al.*[53] or Xu *et al.*[54]). Based on the resistivity behavior, it is also possible that the dominant scattering centers are electron-ionized impurities[55] at temperatures $T \lesssim 100$ K. It is worth mentioning that our results are in good agreement with other measurements done in similar $Bi_{100-x}Sb_x$ thin films[43,56–58], both in magnitude and sign and also in the general temperature dependence.

The performance of thermoelectric (TE) materials is usually characterized by the dimensionless figure of merit $ZT = (S^2/\rho\kappa)T$, where ρ is the electric resistivity, κ is the thermal conductivity and S is the TE power. Consequently, in order to improve the performance of TE materials, it is necessary to increase the TE power factor $PF = S^2/\rho$, which is mainly associated to the electronic part of materials[59]. The temperature-dependent power factors $PF(T)$ for the three studied samples have been obtained from $\rho(T)$ and $S(T)$ results and are shown in the inset of Fig. 4. $PF(T)$ increases with T in the three samples, displaying a maximum near room temperature. This value is particularly high for $Bi_{85}Sb_{15}$ ($\approx 23 \times 10^{-3}$ W/mK^2), compared to other authors results, e.g. those from Malik *et al.*[56], Cho *et al.*[57,58] and Kitagawa *et al.*[43] However, the $S(T)$ results from these works[43,56–58] are very similar to ours, which leads us to conclude that the responsible for the enhancement in $PF(T) = S^2/\rho$ is a decrease in resistivity $\rho(T)$, which is in turn related to
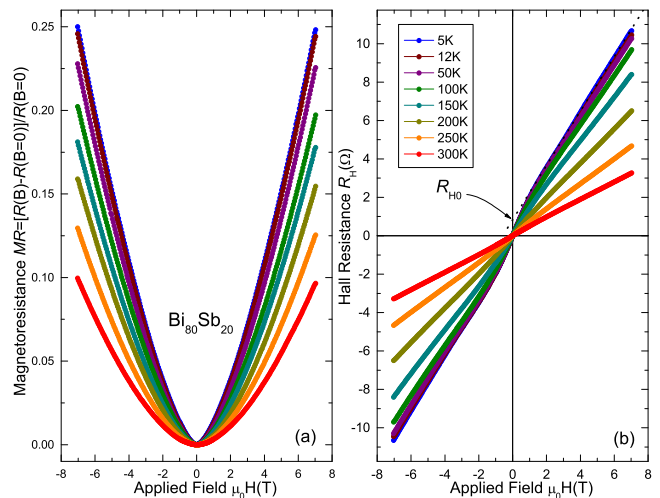
the increase in the electrical conductivity of the surface-dominated transport and thermally activated charge carriers of the bulk.

C. Magnetoresistance and Hall effect

In this Section we present results of the magnetotransport properties measured to our samples in a wide range of temperatures. The magnetoresistance (MR) defined as $MR = [R(B) - R(B = 0)]/R(B = 0)$, and the measured Hall resistance $R_H(B)$ are plotted for samples $Bi_{80}Sb_{20}$, $Bi_{85}Sb_{15}$ and $Bi_{90}Sb_{10}$ in Fig. 5, 6 and 7, respectively.

A positive magnetoresistance in the entire range of investigated temperatures is obtained in every case, being the MR behavior as a function of applied field and temperature strongly dependent on the sample's composition. This becomes clear when plotting $MR(B = 7$ T) vs. T as shown in Fig. 8 where, in order to compare the three samples in the same scale, we have multiplied the results of $Bi_{80}Sb_{20}$ and $Bi_{90}Sb_{10}$ by 10 and 3, respectively. We can observe that in all samples the $MR(B = 7$ T) decreases linearly with T at very different rates. Sample $Bi_{85}Sb_{15}$ displays a remarkable value of $MR(B = 7$ T) of $\sim 600\%$ at 5 K which decreases to $\sim 125\%$ at 300 K. This change in MR is one of the highest reported for polycrystalline TI samples in the same

TABLE III. Results of the fitting parameters using Eq.(5). The Debye temperatures were calculated using Eq.(6).

Sample	E_F(eV)	E_{F0}(eV)	θ_D (K)
$Bi_{80}Sb_{20}$	0.038	10.19	127
$Bi_{85}Sb_{15}$	0.034	10.15	125
$Bi_{90}Sb_{10}$	0.032	10.12	123

Fig. 6. Magnetoresistance (a) and Hall resistance (b) of sample $Bi_{85}Sb_{15}$.

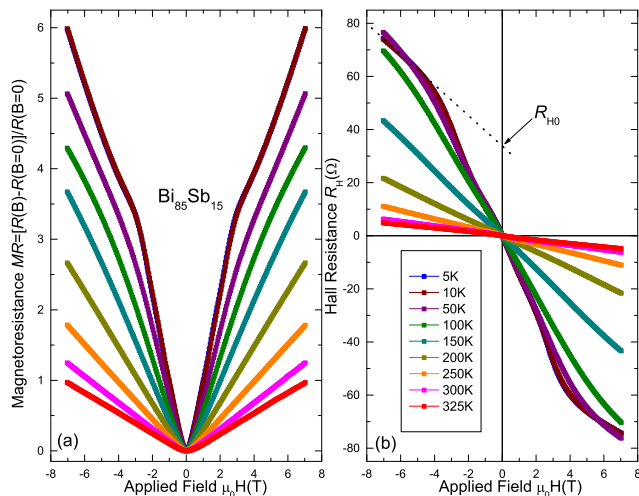Fig. 7. Magnetoresistance (a) and Hall resistance (b) of sample $Bi_{90}Sb_{10}$.

field and temperature ranges[60] and half the measured value obtained for a $Bi_{93}Sb_7$ single crystal[25].

Samples $Bi_{80}Sb_{20}$ and $Bi_{90}Sb_{10}$ show similar MR behavior over the entire measured range of magnetic field and temperature, i.e. an almost $\sim B^2$ dependence due to the Lorenz force contribution on the carriers scattering, under the influence of a perpendicular magnetic field[61]. On the other hand, sample $Bi_{85}Sb_{15}$ displays not only the highest MR values but also the most interesting behavior because it shows a clear trend at temperatures below $T = 75\,K$ and a different one above this point (Fig. 6a). At low temperatures, MR increases almost linearly with the field up to $\mu_0 H \lesssim 3\,T$ and then the system follows a Lorentz behavior. This can be clearly noticed in Fig. 6a and in Fig. 10a, where MR measurements at different temperatures below 50 K are displayed. At temperatures above $T = 75\,K$, MR increases almost linearly in entire range of fields used in our experiments (Fig. 6a).

Maurya $et\ al.$[25] investigated the magnetotransport properties of a $Bi_{97}Sb_3$ single crystal and found that the MR data could not be properly fitted using the Hikami-Larkin-Nagaoka (HLN) model because of the contribution of bulk conductivity, which is not considered in the model. As sample $Bi_{85}Sb_{15}$ displays a similar MR behavior than $Bi_{97}Sb_3$ single crystal, we can expect that the HLN model will not be adequate either.

Hall effect (HE) measurements were performed at the same temperatures as MR experiments. According to our results, the HE sign of sample $Bi_{80}Sb_{20}$ indicates that the majority of carriers are holes, while the behavior of HE in $Bi_{85}Sb_{15}$ and $Bi_{90}Sb_{10}$ indicates that electrons are the carriers in these cases. For the three samples, we can observe that the HE is not linear in the full range of field measured in this work, which is more evident in sample $Bi_{85}Sb_{15}$ at low temperatures. To make this effect more evident and to quantify the change in the slope of the HE, we have used a linear fit to the high field region of the HE
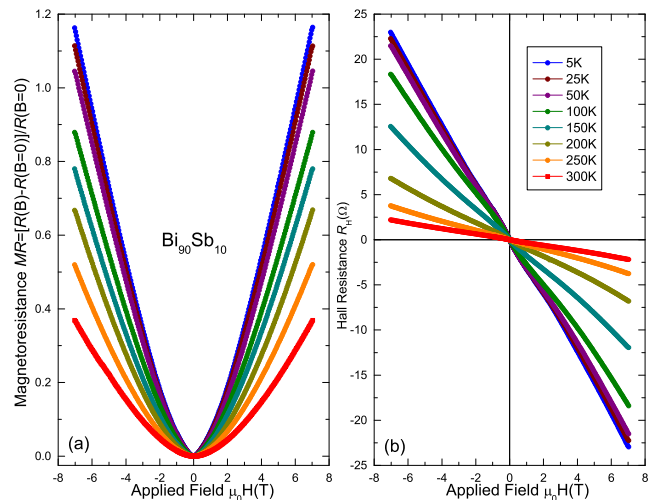
and extrapolated to $\mu_0 H = 0$, such that the $y-$intercept (being the vertical axis R_H) is called R_{H0}. The R_{H0} values obtained from the fits for the three samples are plotted in the inset of Fig. 8a.

Similar values of R_{H0} (below 1 Ω), as well as a similar trend with T in the whole temperature range are obtained for both $Bi_{80}Sb_{20}$ and $Bi_{90}Sb_{10}$. On the other hand, sample $Bi_{85}Sb_{15}$ displays comparable R_{H0} values (between 0.1 and 1 Ω) only at $T \geq 150\,K$. At lower temperatures, R_{H0} reaches values higher than $10\,\Omega$. We interpret this drastic change in the slope of the HE as a consequence of the existence of two types of carriers in this sample. Even when this effect could be accounted for by the anomalous Hall effect (AHE), we disregard this possibility because no signature of magnetic order is detected when measuring MR and HE (Fig. 6). In fact, not a hysteretic HE nor the usual butterfly-shaped MR loops for ferromagnetic materials[61,62] are observed in $Bi_{85}Sb_{15}$.

Two Hall coefficients were calculated from the HE curves, corresponding to the fitting of the low-field (R_{LF}) and the high-field (R_{HF}) data (we have assumed low-field $B < 2\,T$ and high-field $B > 2\,T$), and the results are shown in Fig. 8b. At $T \geq 150\,K$ the absolute values of both R_{LF} and R_{HF} decrease with increasing T and they are almost indistinguishable in each sample. A larger difference between the low-field and the high-field coefficients is observed at $T < 150\,K$, especially in $Bi_{85}Sb_{15}$. To further investigate this behavior, we calculated the 3D carrier density n^{3D} considering two regimes, as in the case of the Hall coefficients, one in the low-field range (n_{LF}^{3D}) and another in the high-field range (n_{HF}^{3D}). The results of the obtained 3D carrier densities are plotted in Fig. 9a, where a similar general trend with T can be observed for the three samples.

It is remarkable that our carrier densities calculated from HE data are in agreement with those from other
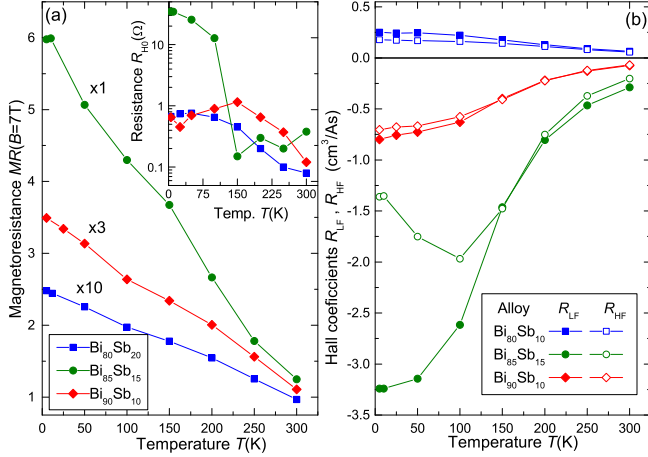
Fig. 8. Magnetoresistance at $B = 7$ T (a) and the estimated Hall coefficients at low R_{LF} and high R_{HF} applied magnetic fields, respectively (b). The inset in (a) shows the residual resistance R_{H0} as defined in the main text. The sizes of the used symbols are chosen in the order of the error bars. The numbers beside the results in (a) are multiplication factors.

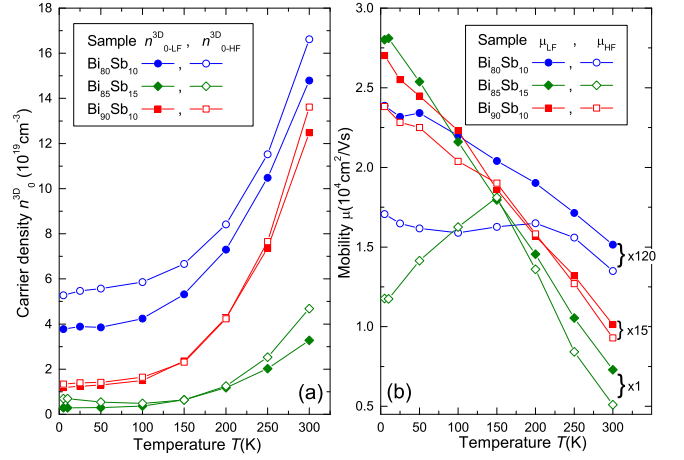

Fig. 9. 3D carrier density $n^{3D}(T)$ (a) and estimated carrier mobility $\mu(T)$ (b). The numbers in (b) are multiplication factors.

works, both in value[14,42,43,57,63] and general temperature dependence[14,43,57,63]. In particular, Taskin and Ando[17] investigated a $Bi_{91}Sb_9$ bulk sample measuring the Hall effect and magnetoresistance. These authors found that $n^{3D} \approx 1.8 \times 10^{17} cm^{-3}$ (from HE) and $n^{3D} \approx 8.1 \times 10^{16} cm^{-3}$ (from quantum oscillations in the MR), being values comparable to our results, especially the one coming from the HE.

The carriers mobility, defined as

$$\mu(T) = \frac{1}{|e|\rho(T)\,n^{3D}(T)} \, ,$$

was calculated for our samples in the low-field and in the high-field regimes, and the results are plotted in Fig. 9b. In order to compare the values of the three samples using the same scale, we have multiplied the mobilities of $Bi_{80}Sb_{20}$ ($f = 120$) and $Bi_{90}Sb_{10}$ ($f = 15$) by a factor f. It is evident from the graph that sample $Bi_{85}Sb_{15}$ has the highest mobility by one or two orders of magnitude.

The mobilities calculated using data from the low-field range $\mu_{LF}(T)$ display a rather linear behavior with a negative slope, in the three investigated samples. The same is true for $\mu_{HF}(T)$ in $Bi_{80}Sb_{20}$ and $Bi_{90}Sb_{10}$ but sample $Bi_{85}Sb_{15}$ presents a change in slope below 150 K, mimicking the trend observed in the Hall coefficients (Fig. 8b). We interpret that this behavior is originated in the strong metallic component of this sample in the same range of temperatures.

The values and temperature dependence of the mobilities obtained in this work are in good agreement with results from other works on BiSb thin films[42,43,60,63] and in bulk[14]. It is noteworthy that the carrier mobility of sample $Bi_{85}Sb_{15}$ of $\mu \approx 2.8 \times 10^4 cm^2/Vs$ and

$\mu \approx 0.72 \times 10^4 cm^2/Vs$ at 5 and 300 K respectively, are comparable to mobilities of other TI materials such as Bi_2Se_3[24,64,65] and Bi_2Te_3[66,67].

D. Quantum oscillations

The large metallic contribution to $R(T)$, the linear behavior of $MR(B)$ and the MR huge changes observed at low temperatures in $Bi_{85}Sb_{15}$ lead us to conclude that there exists a topologically protected surface-state in this sample. Clear evidence of a 2D metallic state in TI materials is the observation of quantum oscillations in MR at low temperatures, known as the Shubnikov-de Haas (SdH) oscillations, as already observed in TI $Bi_{100-x}Sb_x$ samples[17,18,31,68]. In order to investigate the presence of SdH oscillations in our $Bi_{85}Sb_{15}$ film, we have measured MR in small ΔT steps (Fig. 10a) and followed the usual procedure to make the quantum oscillations visible, that is to plot the first derivative of MR vs. the inverse of the applied magnetic field (Fig. 10b).

As depicted in Fig. 10b, periodic oscillations are evident which disappear with increasing temperature; in our case, the effect is lost at $T \geq 21$ K. A main oscillation with a period of $\Delta \approx 0.26\,T^{-1}$ can be observed. From this frequency it is possible to estimate the two dimensional (2D) carrier density using the equation $n_{2D} = 2e/h\Delta$, being h Planck's constant. Thus, for sample $Bi_{85}Sb_{15}$ we obtained a 2D carrier density $n_{2D} = 2.96 \times 10^{10} cm^{-2}$, which is of the same order of magnitude as the 2D carrier density observed in bulk $Bi_{91}Sb_9$ by Taskin and Ando ($n_{2D} = 1.4 \times 10^{10} cm^{-2}$)[17,18], and one order less than reported values for a $Bi_{97}Sb_3$ bulk sample ($n_{2D} = 2.4 \times 10^{11} cm^{-2}$) by Maurya et al[25].

We observe strong quantum oscillations of the magnetoresistance in our $Bi_{85}Sb_{15}$ thin film, originating from a Fermi surface which has a clear two-dimensional charac-
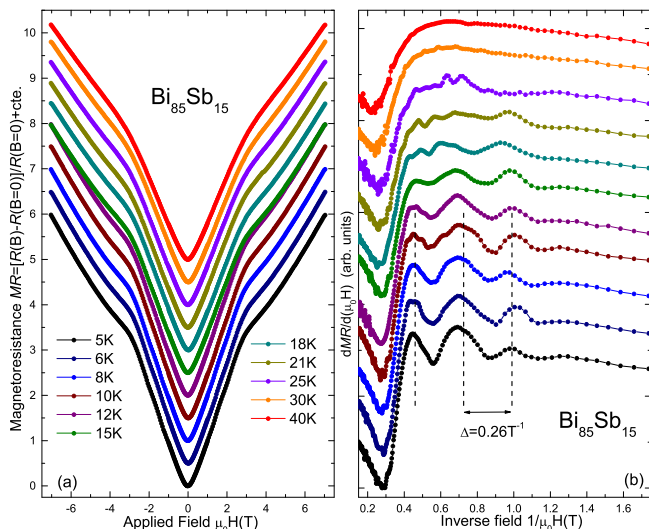
Fig. 10. Magnetoresistance vs. applied magnetic field measured at temperatures below 50 K for sample $Bi_{85}Sb_{15}$ (a). First derivative of MR vs. the inverse applied magnetic field (b). The curves in (a) and (b) were shifted by a constant for the sake of clarity.

ter; these results, in our opinion, support our statement that sample $Bi_{85}Sb_{15}$ presents clear TI properties at low temperatures. In order to further support this affirmation, we calculated the Berry phase β, which is an important parameter to prove the existence of topological surface states. The surface state electrons are bulk state electrons and should have $\beta = 0$, whereas $\beta = 0.5$ for Dirac Fermions. The Berry phase β can be experimentally determined from the SdH oscillations[69] by analyzing the so-called Landau-level (LL) fan diagram. According to the literature, when a linear fit to the LL fan diagram is extrapolated to $1/B_N \to 0$, the intercept on the N-index axis gives the phase factor β. As a consequence, when the value thus obtained is $1/2$, it is possible to conclude that the SdH oscillations come from Dirac fermions. Using the SdH oscillations obtained at $T = 5\,\mathrm{K}$ for $Bi_{85}Sb_{15}$ we obtained the fan diagram, which is shown in Fig. 11a. While constructing the LL fan plot, the maxima and minima positions of quantum oscillations in dMR/dB are assigned integer (N) and half-integer numbers $(N + 1/2)$, respectively. In the limit $1/B_N \to 0$ we obtain $\beta = 0.41 \pm 0.03$, which is very close to the theoretical value of 0.5 for Dirac particles. This result further confirms that the observed quantum oscillations originate from topological surface states in our $Bi_{85}Sb_{15}$ thin film. The cyclotron effective mass m_c was also obtained by fitting the normalized experimental $R_T(T)$ of maximum amplitude corresponding to the dMR/dB oscillations, using the standard Lifshitz-Kosevich theory[70]:

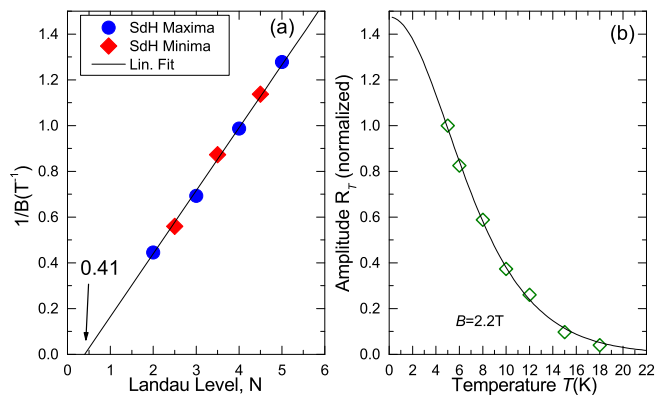$$R_T(T) = R_o \frac{2\pi^2 k_B T/\hbar\omega_c}{\sinh(2\pi^2 k_B T/\hbar\omega_c)}, \qquad (7)$$

Fig. 11. LL fan diagram for sample $Bi_{85}Sb_{15}$, based on the dMR/dB data at $T = 5\,\mathrm{K}$ (a) . Temperature dependence of the amplitude R_T of SdH oscillations at $B = 2.2\,\mathrm{T}$ (b). The solid line corresponds to the fit using Eq. 7.

where

$$R_o = 4\,\exp(-2\pi^2 k_B T_D/\hbar\omega_c), \qquad (8)$$

with $\omega_c = eB/cm_c$, the Dingle temperature $T_D = \hbar/2\pi k_B\tau$ and τ the scattering time. The fit results are shown as a solid line in Fig. 11b, and from the obtained parameters the cyclotron mass is $m_c \approx 0.048\,m_e$, being m_e the free electron mass. Such a small value obtained for m_c is the reason why it is possible to observe pronounced SdH oscillations at relatively low magnetic fields. The obtained Dingle temperature is $T_D = 3.1\,\mathrm{K}$, which corresponds to $\tau = \hbar/(2\pi k_B T_D) = 3.9 \times 10^{-13}$ s. In a next step we can calculate the Fermi velocity $v_F = \hbar k_F^{2D}/m_c$, with $k_F^{2D} = (4\pi n_{2D})^{1/2} = 1.73 \times 10^8\,\mathrm{m^{-1}}$, so we get $v_F = 4.15 \times 10^5$ m/s, similar to the ARPES results of Hsieh et-al [6] for the electron surface bands surrounding the $\bar{\Gamma}$ $(3.7 \times 10^5\mathrm{m/s})$ and $\bar{M}$ $(4.9 \times 10^5\mathrm{m/s})$ points, and a mean-free path $l^{2D} = v_F\tau = 162$ nm. These results are in good agreement with the work of Taskin and Ando[17,18] on a $Bi_{91}Sb_9$ bulk sample $(m_c = 0.0057m_e, T_D = 6.7\,\mathrm{K}, \tau = 1.8 \times 10^{-13}$ s, $k_F^{2D} = 4.15 \times 10^7$ m, $v_F = 8.5 \times 10^5$ m/s, $l^{2D} = 150$ nm.) The experimental results presented in this work, the parameters obtained after analysis and the good agreement with results from other authors, lead us to conclude that the observed quantum oscillations in our $Bi_{85}Sb_{15}$ thin film are of 2D character, i.e. due to a topologically protected surface state which is characteristic of a topological insulator.

IV. CONCLUSION

Polycrystalline thin films of compositions $Bi_{80}Sb_{20}$, $Bi_{85}Sb_{15}$ and $Bi_{90}Sb_{10}$ were successfully prepared using a simple and inexpensive method, which is also versatile and applicable to the production of other technologically interesting materials. SEM images show that the grain

size of all samples are in the order of $\approx 50\,\text{nm}$, EDX results show good agreement with the nominal atomic composition and no presence of ferromagnetic contaminants and the estimated lattice parameters from X-ray results show good agreement with those from the literature.

Resistivity $\rho(T)$, thermopower $S(T)$, power factor $PF(T)$, magnetoresistance $MR(B)$, Hall mobility $\mu(T)$ and carrier density $n^{3D}(T)$ measured in our investigated samples are in complete qualitative and quantitative agreement with similar results from other authors.

Because of the metallic resistivity, huge magnetoresistance, Shubnikov-de Haas oscillations and Berry phase calculation, we have proved that the SdH oscillations observed in $Bi_{85}Sb_{15}$ arise from topological surface states in this sample. Several physical parameters characterizing the topological surface states were estimated using the Lifshitz-Kosevich theory and they are in agreement with those from the literature.

In this work, a fitting model that considers separately the bulk and surface contributions to the resistivity was used for the first time, giving fitting parameters that reflect the expected experimental values and thus, can be applied for future studies on other TI materials. We attribute the clear TI behavior observed in our polycrystalline $Bi_{85}Sb_{15}$ thin film to the extraordinary property of the topologically protected surface states, which are robust against structural disorder, e.g. the grain boundaries of our polycrystalline material.

The simplicity, versatility, low-cost preparation and high quality of TI materials produced through sequential flash evaporation can motivate the use of this synthesis method to obtain other binary and ternary topological insulators such as Bi_2Te_3, Bi_2Te_2Se, Sb_2Te_2Se, $PbSb_2Te_4$, Weyl semimetals such as WTe_2 and NbAs, and others.

* e.osmic@hzdr.de; †Present Address: High Field Magnetic Laboratory Dresden (HLD-EMFL), Helmholtz Center Dresden-Rossendorf, D-01328 Dresden, Germany

[1] L. Fu, C. L. Kane, and E. J. Mele, Phys. Rev. Lett. **98**, 106803 (2007).

[2] L. Fu and C. L. Kane, Phys. Rev. B **76**, 045302 (2007).

[3] M. Liu, J. Zhang, C.-Z. Chang, Z. Zhang, X. Feng, K. Li, K. He, L.-L. Wang, X. Chen, X. Dai, Z. Fang, Q.-K. Xue, X. Ma, and Y. Wang, Phys. Rev. Lett. **108**, 036805 (2012).

[4] J. E. Moore and L. Balents, Phys. Rev. B **75**, 121306(R) (2007).

[5] D. Hsieh, Y. Xia, L. Wray, D. Qian, A. Pal, J. H. Dil, J. Osterwalder, F. Meier, G. Bihlmayer, C. L. Kane, Y. S. Hor, R. J. Cava, and M. Z. Hasan, Science **323**, 919 (2009).

[6] D. Hsieh, D. Qian, L. Wray, Y. Xia, Y. S. Hor, R. J. Cava, and M. Z. Hasan, Nature (London) **452**, 970 (2008).

[7] Y. Xia, D. Qian, D. Hsieh, L. Wray, A. Pal, H. Lin, A. Bansil, D. Grauer, Y. S. Hor, R. J. Cava, and M. Z. Hasan, Nat. Phys. **5**, 398 (2009).

[8] H. Zhang, C. Liu, X. Qi, X. Dai, Z. Fang, and S. Zhang, Nat. Phys **5**, 438 (2009).

[9] Y. L. Chen, J. G. Analytis, J.-H. Chu, Z. K. Liu, S.-K. Mo, X. L. Qi, H. J. Zhang, D. H. Lu, X. Dai, Z. Fang, S. C. Zhang, I. R. Fisher, Z. Hussain, and Z.-X. Shen, Science **325**, 178 (2009).

[10] J. Tian, I. Childres, H. Cao, T. S. I. Miotkowski, and Y.-P. Chen, Solid State Communications **191**, 1 (2014).

[11] X.-L. Qi and S.-C. Zhang, Rev. Mod. Phys. **83**, 1057 (2011).

[12] B. Lian, X.-Q. Sun, A. Vaezi, X.-L. Qi, and S.-C. Zhang, Proc. Natl. Acad. Sci. U.S.A **115**, 10938 (2018).

[13] D. Schoenberg and M. Z. Uddin, Proc. R. Soc. London A **156**, 687 (1936).

[14] A. L. Jain, Phys. Rev. **114**, 1518 (1959).

[15] B. Lenoir, A. Dauscher, M. Cassart, Y. I. Ravich, and H. Scherrer, J. Phys. Chem. Solids **59**, 129 (1998).

[16] B. Lenoir, M. Cassart, J. P. Michenaud, H. Scherrer, and S. Scherrer, J. Phys. Chem. Solids **57**, 89 (1996).

[17] A. A. Taskin and Y. Ando, Phys. Rev. B **80**, 085303 (2009).

[18] A. A. Taskin, K. Segawa, and Y. Ando, Phys. Rev. B **82**, 121302(R) (2010).

[19] S. Hikami, A. Larkin, and Y. Nagaoka, Prog. Theor. Phys. **63**, 707 (1980).

[20] K. Nomura, M. Koshino, and S. Ryu, Phys. Rev. Lett. **99**, 146806 (2007).

[21] L. Bao and et al, Sci. Rep. **2**, 2012 (726).

[22] W. Ning, H. Du, F. Kong, J. Yang, Y. Han, M. Tian, and Y. Zhang, Sci. Rep **3**, 1564 (2013).

[23] J. Cha, M. Claassen, D. Kong, S. Hong, K. Koski, X.-L. Qi, and Y. Cui, Nano Letters **12**, 4355 (2012).

[24] J. Barzola-Quiquia, T. Lehmann, M. Stiller, D. Spemann, P. Esquinazi, and P. Häussler, J. Appl. Phys. **117**, 075301 (2015).

[25] V. K. Maurya, M. M. Patidar, A. Dhaka, R. Rawa, V. Ganesan, and R. S. Dhaka, Phys. Rev. B **102**, 144412 (2020).

[26] G. Zhang and et al., Adv. Funct. Mater. **21**, 2351 (2011).

[27] M.-X. Wang and et al., Science **336**, 52 (2012).

[28] Y.-F. Lin and et al., J. Phys. Chem. C **111**, 18538 (2007).

[29] J. Checkelsky and et al., Phys. Rev. Lett. **103**, 246601 (2009).

[30] D. Hsie and et al., Nature **460**, 1101 (2009).

[31] A. Nikolaeva, L. Konopko, T. Huber, I. Popov, P. Bodiul, and E. Moloshnik, Phys. Status Solidi A **211**, 1325 (2014).

[32] W. Jiao, S. Jiang, C. Feng, Z. Xu, G. Cao, M. Xu, D. Feng, A. Yamada, K. Matsubayashi, and Y. Uwatoko, AIP Advances **2**, 022148 (2012).

[33] P. Häussler, Topics Appl. Phys. **72**, 163 (1994).

[34] C. Roth, G. Schwalbe, R. Knöfler, F. Zavaliche, O. Madel, R. Haberkern, and P. Häussler, Journal of Non-Crystalline Solids **252**, 869 (1999).

[35] R. Haberkern, J. Barzola-Quiquia, C. Madel, and P. Häussler, MRS Proceedings **643**, 643 (2001).

[36] J. Barzola-Quiquia, M. Stiller, M. Stiehler, P. Esquinazi, and P. Häussler, Mater. Res. Express **2**, 096403 (2015).

[37] R. H. amd K. Khedhri, C. Madel, and P. Häussler, Materials Science and Engineering , 294 (2000).

[38] J. Barzola-Quiquia, M. Stiller, P. D. Esquinazi, J. Quispe-Marcatoma, and P. Häussler, J. Magn. Magn. Mater. **456**, 281 (2018).

[39] E. Compans, Rev. Sci. Instrum. **60**, 2715 (1989).

[40] J. P. Dismukes, R. J. Paff, R. T. Smith, and R. Ulmer, Journal of Chemical and Engineering Data **13**, 317 (1968).

[41] F. Völklein and E. Kessler, Phys. Stat. Sol. B **134**, 351 (1986).

[42] C. H. Will, M. T. Elm, P. J. Klar, B. Landschreiber, E. Güne, and S. Schlecht, J. Appl. Phys. **114**, 193707 (2013).

[43] H. Kitagawa, H. Noguchi, T. Kiyabu, M. Itoh, and Y. Noda, J. Phys. Chem. Solids **65**, 1223 (2004).

[44] M. Zoraghi, J. Barzola-Quiquia, M. Stiller, A. Setzer, P. Esquinazi, G. H. Kloess, T. Muenster, T. Lühmann, and I. Estrela-Lopis, Phys. Rev. B **95**, 045308 (2017).

[45] J. Barzola-Quiquia, J.-L. Yao, P. Rödiger, K. Schindler, and P. Esquinazi, J. Phys. Chem. Solids **59**, 129 (1959).

[46] J. Barzola-Quiquia, A. Ballestar, S. Dusari, and P. Esquinazi, "Experimental study of the intrinsic and extrinsic transport properties of graphite and multigraphene samples," (Intech, Open Access Publisher, Jian Ru Gong (ed.), 2011) Chap. 8, ISBN 978-953-307-292-0.

[47] M. Zoraghi, J. Barzola-Quiquia, M. Stiller, P. D. Esquinazi, and I. Estrela-Lopis, Carbon **139**, 1074 (2018).

[48] N. Garcia, P. Esquinazi, J. Barzola-Quiquia, and S. Dusari, New J. Phys. **14**, 053015 (2012).

[49] K. Malik, D. Das, D. Mondal, D. Chattopadhyay, A. K. Deb, S. Bandyopadhyay, and A. Banerjee, J. Appl. Phys. **112**, 083706 (2012).

[50] J. Barzola-Quiquia, C. Lauinger, M. Zoraghi, M. Stiller, S. Sharma, and P. Häussler, Supercond. Sci. Technol. **30**, 015013 (2017).

[51] Y. Onose, R. Y. A. Tsukazaki, H. Yuan, T. Hidaka, Y. Iwasa, M. Kawasaki, and Y. Tokura, Appl. Phys. Express **4**, 083001 (2011).

[52] J. G. Analytis, J.-H. Chu, Y. Chen, F. Corredor, R. D. McDonald, Z. X. Shen, and I. R. Fisher, Phys. Rev. B **81**, 205407 (2010).

[53] O. A. Tretiakov, A. Abanov, and J. Sinova, J. Appl. Phys. **111**, 07E319 (2012).

[54] Y. Xu, Z. Gan, and S.-C. Zhang, Phys. Rev. Lett. **112**, 226801 (2014).

[55] Y. V. Ivanov, A. T. Burkov, and D. A. Pshenay-Severin, Phys. Status Solidi B **255**, 1800020 (2018).

[56] K. Malik, D. Das, S. Bandyopadhyay, P. Mandal, A. K. Deb, V. Srihari, and A. Banerjee, Appl. Phys. Lett. **103**, 242108 (2013).

[57] S. Cho, A. DiVenere, G. K. Wong, J.-B. Ketterson, and J.-R. Meyer, J. Appl. Phys. **85**, 3655 (1999).

[58] S. Cho, A. DiVenere, G.-K. Wong, J.-B. Ketterson, and J.-R. Meyer, Phys. Rev. B **59**, 10691 (1999).

[59] D. J. Bergman and L. G. Fel, J. Appl. Phys. **85**, 8205 (1999).

[60] D. Das, K. Malik, S. Bandyopadhyay, D. Das, S. Chatterjee, and A. Banerjee, Appl. Phys. Lett. **105**, 082105 (2014).

[61] C. Hurd, *The Hall effect in Metals and Alloys* (Plenum New York, 1972).

[62] J. Barzola-Quiquia, A. Lessig, A. Ballestar, C. Zandalazini, G. Bridoux, F. Bern, and P. Esquinazi, J. Phys.: Condens. Matter **24**, 366006 (2012).

[63] I. Vurgaftman, J. R. Meyer, C. A. Hoffman, S. Cho, A. DiVenere, G. K. Wong, and J. B. Ketterson, J. Phys.: Condens. Matter **11**, 5157 (1999).

[64] Y. Yan, L.-X. Wang, D.-P. Yu, and Z.-M. Liao, Appl. Phys. Lett. **103**, 033106 (2013).

[65] O. Chiatti, C. R. D. Lawrenz, M. Busch, S. Dusari, J. Sanchez-Barriga, A. Mogilatenko, L. V. Yashina, S. V. A. A. U. O. Rader, and S. F. Fischer, Sci. Rep. **6**, 27483 (2016).

[66] Y.-Y. Li, G. Wang, X.-G. Zhu, M.-H. Liu, C. Ye, X. Chen, Y.-Y. Wang, K. He, L.-L. Wang, X.-C. Ma, H.-J. Zhang, X. Dai, Z. Fang, X.-C. Xie, Y. Liu, X.-L. Qi, J.-F. Jia, S.-C. Zhang, and Q.-K. Xue, Adv. Mater. **22**, 4002 (2010).

[67] M. Samanta, K. Pal, and U. V. W. und K. Biswas, Angew. Chem. **132**, 4852 (2020).

[68] A. Banerjee, B. Fauque, K. Izawa, A. Miyake, I. Sheikin, J. Flouquet, B. Lenoir, and K. Behnia, Phys. Rev. B **78**, 161103(R) (2008).

[69] G. P. Mikitik and Y. V. Sharlai, Phys. Rev. Lett. **82**, 2147 (1999).

[70] D. Shoenberg, *Magnetic Oscillations in Metals* (Cambridge University Press, Cambridge,, 1984).

Supplementary information to: Thermopower and magnetotransport properties of $Bi_{100-x}Sb_x$ topological insulator thin films prepared by flash evaporation

E. Osmic,[1, *] J. Barzola-Quiquia,[1] W. Böhlmann,[1] P. G. Bercoff,[2] L. Venosta,[2] and P. Häussler[3]

[1] *Felix-Bloch Institute for Solid-state Physics, University of Leipzig, 04103 Leipzig, Germany*
[2] *Universidad Nacional de Córdoba, Facultad de Matemática, Astronomía, Física y Computación (FAMAF).*
Instituto de Física Enrique Gaviola (IFEG), CONICET.
Av. Medina Allende s/n, 5000 Córdoba, Argentina
[3] *Division of Thin Films Physics, Institute of Physics,*
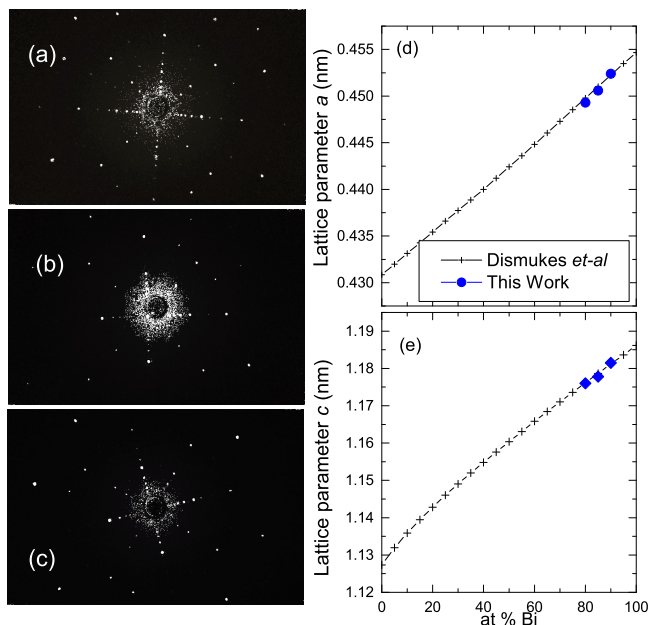*Chemnitz University of Technology, 09107 Chemnitz, Germany*
(Dated: February 11, 2022)

Fig. S 1. Laue diffraction results, for (a) $Bi_{80}Sb_{20}$, (b) $Bi_{85}Sb_{15}$ and (c) $Bi_{90}Sb_{10}$. The lattice parameters a and c obtained from the results shown in (a)-(c) are displayed in (d) and (e). The results displayed with symbols + in (d) and (e) are taken from the work by Dismukes *et al.* [1].

I. X-RAY DIFFRACTION

X-ray Laue diffraction was performed using a Inel EQUINOX 3000 X-ray diffractometer. The experiments were performed at room temperature on the same samples used in this work, after measuring the transport properties. The Laue patterns are shown in Fig. S1 from (a) to (c). Fig. S1 (d) and (e) present the lattice parameters values obtained from the Laue patterns analysis together with similar results reported by Dismukes *et al.* for the whole range of the alloy compositions. From this comparison it is evident that our results are in good agreement whith the expected lattice parameters for the corresponding phase. Another conclusion that can be drawn from these measurements is that our films have
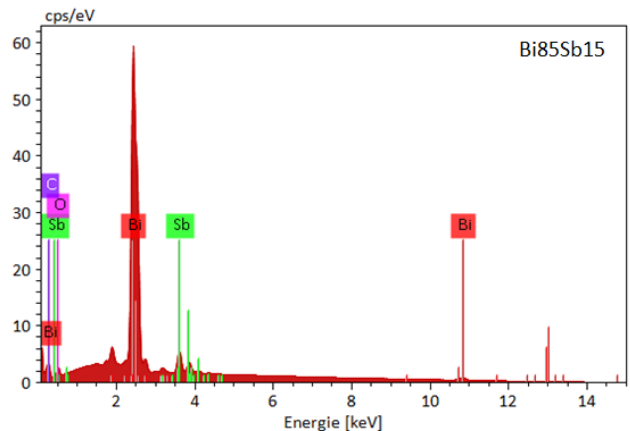

Fig. S 2. EDX spectrum obtained for sample $Bi_{90}Sb_{10}$.

the c-axis oriented perpendicular to the plane of the substrate, while a, b-axes are randomly oriented parallel to the substrate plane, thus implying that during our experiments the magnetic field was applied parallel to the c-axis.

II. ENERGY-DISPERSIVE X-RAY SPECTROSCOPY

Elemental analysis was performed using the energy-dispersive X-ray (EDX) spectrometer included in a FEI NanoLab XT 200 dual-beam microscope. The experiments were done at room temperature after the trans-

Element	Mass [%]	Mass. Norma. [%]	Atom [%]	Abs. Error [%]
Bismuth	78.1	87.4	62.9	1.2
Antimony	9.1	10.2	12.6	0.1
Oxygen	1.5	1.7	15.7	0.1
Carbon	0.6	0.7	8.8	0.1

TABLE I. Elemental composition of sample $Bi_{85}Sb_{15}$.

Fig. S 3. EDX spectraum obtained for sample $Bi_{90}Sb_{10}$.

overview on the chemical composition is given in Table I for $Bi_{85}Sb_{15}$ and in Table II for $Bi_{90}Sb_{10}$. Considering these results it is possible to state that our films do not contain any ferromagnetic contaminants (such as Fe, Co or Ni) within the detection limits of this technique. The presence of silicon and oxygen is originated from the substrate (silicon substrate caped with amorphous SiO_2), while carbon is attributed to the sample holder or some remaining solvent used while removing from the cryostat holder. However, the small amounts of these elements do not interfere or play any role on the transport properties of the films. Besides confirming the absence of ferromagnetic impurities, EDX analysis allowed also to verify that the actual composition of the samples agrees with the nominal value with an error of of $\pm 1\%$, confirming that our synthesis method (flash evaporation) is very accurate to produce the desired compositions.

port measurements were performed. We present results of samples $Bi_{85}Sb_{15}$ and $Bi_{90}Sb_{10}$.

The main aim of this experiment was to confirm the nominal composition of the films and to determine if ferromagnetic contaminants were present in the samples. EDX spectra corresponding to samples $Bi_{85}Sb_{15}$ and $Bi_{90}Sb_{10}$ are presented in Fig. S2 and Fig. S3, respectively. Using a standard EDX analysis program, the scanned spectra were analyzed, the peaks were identied and the weight and atomic percentage of the measured elements were calculated with the ZAF protocol. An

Element	Mass [%]	Mass. Norma. [%]	Atom [%]	Abs. Error [%]
Bismuth	73.1	88.8	54.2	1.1
Antimony	4.8	5.9	6.1	0.1
Silicon	1.6	1.9	8.9	0.1
Oxygen	1.6	1.9	15.2	0.1
Carbon	1.2	1.5	15.6	0.1

TABLE II. Elemental composition of sample $Bi_{90}Sb_{10}$.

* e.osmic@hzdr.de; †Present Address: High Field Magnetic Laboratory Dresden (HLD-EMFL), Helmholtz Center Dresden-Rossendorf, D-01328 Dresden, Germany

[1] J. P. Dismukes, R. J. Paff, R. T. Smith, and R. Ulmer, Journal of Chemical and Engineering Data **13**, 317 (1968).